BRNO UNIVERSITY OF TECHNOLOGY
VYSOKÉ UČENÍ TECHNICKÉ V BRNĚ

FACULTY OF ELECTRICAL ENGINEERING AND COMMUNICATION
FAKULTA ELEKTROTECHNIKY
A KOMUNIKAČNÍCH TECHNOLOGIÍ

DEPARTMENT OF RADIO ELECTRONICS
ÚSTAV RADIOELEKTRONIKY

REVERBERATION REDUCTION IN TRANSFORMER-LESS ULTRASONIC SENSORS FOR PARKING APPLICATIONS
POTLAČENÍ DOZVUKŮ U BEZTRANSFORMÁTOROVÝCH ULTRAZVUKOVÝCH SNÍMAČŮ PRO PARKOVACÍ ÚČELY

DOCTORAL THESIS
DIZERTAČNÍ PRÁCE

AUTHOR Ing. Jan Ledvina
AUTOR PRÁCE

SUPERVISOR doc. Dr. Ing. Pavel Horský
ŠKOLITEL

BRNO 2021

KEYWORDS

Grounded inductance simulator, Ultrasonic sensor, Reverberation reduction, Ring-down measurement, Transducer damping, Transducer adaptability.

KLIČOVÁ SLOVA

Dozvukové měření, Uzemněný simulátor indukčnosti, Ultrazvukový snímač, Potlačení reverberací, Tlumení měniče, Přizpůsobení na měnič.

THESIS IS AVAILABLE AT

Dept. of Radio Electronics

Faculty of Electrical Engineering and Communication

Brno University of Technology

Technická 3082/12,

616 00 Brno

The Czech Republic.

CONTENTS

1 INTRODUCTION AND SETTING GOALS

A tremendous technological advancement lead into introduction of terms such as a self-driving car, an autonomous vehicle, an intelligent vehicle, a smart car, a driver-less vehicle, and many others. In a sense, they are all linked to a vision of having a vehicle that can operate on its own (no human input) in all conditions. To enable such vehicles a large variety of sensors is needed. In general, each type of sensor has its advantages and disadvantages, which makes it suitable for certain type of applications. This is often documented by infographics depicting a car with different sensors for various assistants, example of such a graphic is in Fig. 1.1.

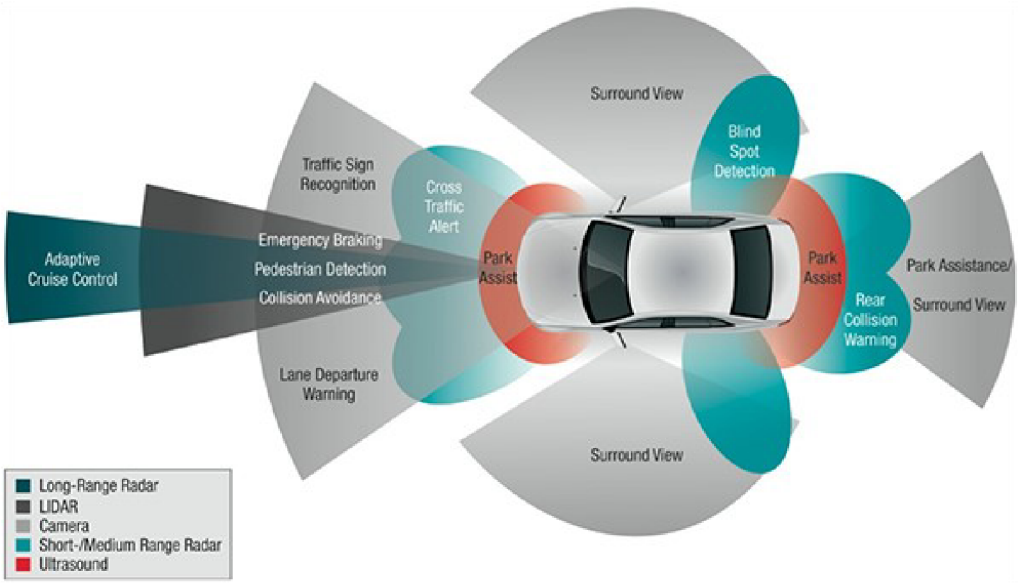

Fig. 1.1 Infographic showing vehicle sensing fields for different assistants (taken from [1])

A specific task associated with passenger vehicles is parking. Unlike a regular driving on a motorway, the parking usually takes place in slow speeds and in a limited space. The main specific is the need to cover completely the close surroundings, which is almost impossible with just a single sensor. Instead, sensor arrays or cooperation of multiple different sensors is often employed.

In most PAS implementations, an Ultrasonic Sensor (ULS) is used to measure a distance to an obstacle [2], [3], and [4]. The reason why ULS is used in PAS is due to its good short ranging, robustness to weather, compactness, and cost [5], [6], [7], [8], [9], [10]. The limited long ranging of the ULS still meets the PAS needs. The cost aspect and mechanical constrain are the reasons to use mainly a single transducer configuration for the ULS. The compactness and low cost also enable use of multiple ULS on the same vehicle. The plurality of ULS together with short ranging performance is what makes it the best choice for the PAS.

Typical ULS comprises of a piezoceramic disc attached to a membrane, a mechanical housing, and a control electronic. To miniaturize the ULS, majority of the electronic is integrated in an Application Specific Integrated Circuit (ASIC). Not integrated to the ASIC is typically a transformer. Recently, a transformer-less solution is investigated. Transformer-less solution reduces sensitivity to a magnetic field and allows further reduction of external components. However, elimination of the transformer brings two significant challenges.

The transformer two key functions are boosting the voltage during the transmitting process and damping transducer reverberation. The voltage boosting (typically to 100 V [11]) is needed to maximized power output from the ULS, which is important for the long ranging. On the other hand, reverberation damping is important for short ranging.

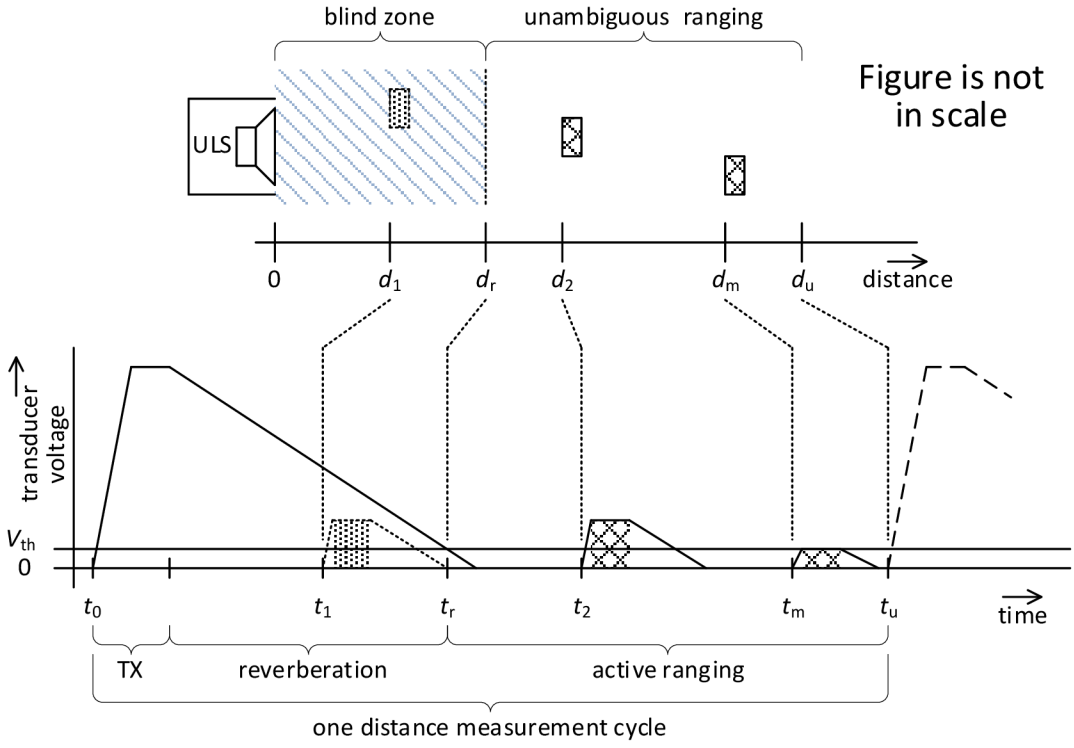

Fig. 1.2 Distance measurement cycle for ULS with single transducer

The reverberation occurs after the transducer has been driven. It is a mechanical self oscillation, in another context also referred to as a ring-down. If the single transducer configuration is used, reverberation can mask out an incoming echo. The consequence is existence of a blind zone, sometimes also referred to as a blind window. The blind zone means the ULS is unable to measure the distance. Unfortunately, the blind zone directly limits the short ranging, which is probably the most important feature of the ULS in the PAS. To better understand the effect of blind zone Fig. 1.2 describes a typical distance measurement cycle in case of ULS with the single transducer. Typically, the blind zone ranges up to 40 cm. Custom tuned circuits

can have the blind zone only 15 cm or less. This difference in ranging indicates the amount of margin, which is needed in large volume production if parameter variation is to be covered.

1.1 Thesis Objectives

From the previous it is obvious, that one of the main limiting factors is the blind zone. Consequently, it is desirable to focus innovative effort on reduction of the blind zone. More accurately, development of transducer damping methods that are less sensitive to the transducer parameter variation. This means the thesis research focus is on reverberation reduction and adaptive damping techniques for transformer-less ULS configuration, with the main objective to demonstrate working transformer-less ULS concept.

2 DAMPING CONCEPTS

A thesis starting point was a literature review that showed interesting field of structural damping [12]. In this field, many nonlinear damping techniques exist [13], [14], unfortunately, majority of these techniques works at relatively low frequencies (~100 Hz). The low frequency allows use of complex digital processing, which is not feasible since the ULS operating frequency is more than 300 times higher. In [14], a nonlinear method called Variable Structure Control (VSC) was used to improve fast transients on the transducer. However, its use for the transducer damping is not feasible due to the damping requirements on the dynamic range.

Consequently, investigation of theoretical damping concepts was needed. Two key concepts explored are nonlinear damping methods for transformer-less ULS and adaptively tuned linear shunts for transformer-less damping. To help with this activity, a benchmark transducer is also defined.

2.1 Definition of Benchmark Transducer

Suppose one is to develop a new damping concept, then it is desirable not to shape it towards a single transducer type but rather make it as universal as possible. For this purpose, Table 2.1 presents limits that cover a large portion of currently used transducers. These limits form a parameter space of a virtual benchmark transducer. The virtual benchmark transducer with its wide limits can be used for our evaluations later. It should be noted that such a table will always differ depending on how we select initial transducer samples.

Table 2.1 Definition of benchmark transducer limits

Parameter	Min①	Max①	Note
f_{m0}	44 kHz (35)	69 kHz (70)	
C_p	0.8 nF (0.7)	7 nF	
Q_{m0}	10	70	
R_{m0}			Calculate from f_{m0}, L_{m0}, and Q_{m0}
L_{m0}	30 mH	600 mH	
C_{m0}			Calculate from f_{m0}, L_{m0}

① values in brackets were added later as more transducers were examined

The Table 2.1 does not specify parameter C_{m0} directly, but rather through additional equation that works with transducer resonant frequency. This is more

meaningful way how to specify the value for the model. Similarly, the R_{m0} is specified with a quality factor (Q-factor). In this way, the R_{m0} is

$$R_{\mathrm{m0}} = 2\pi f_{m0} L_{m0} Q_{m0}. \tag{2.1}$$

Similarly, table specifies C_{m0} as

$$C_{\mathrm{m0}} = \frac{1}{(2\pi f_{m0})^2 L_{m0}}. \tag{2.2}$$

2.2 Nonlinear Damping Concepts

One can ask a question how to achieve the ideal nonlinear damping. It can be shown that ideal generic damping should always transfer energy from the transducer motional branch, meaning transducer power bilance is always negative. This implies transducer voltage and motional current zerocrossings must be alligned. In principle, this observation can be used to state following damping condition

$$v_{\mathrm{transducer}}(t) = \begin{cases} V_{\mathrm{damp}}, & \text{if } i_{\mathrm{m0}}(t) < 0 \\ -V_{\mathrm{damp}}, & \text{if } i_{\mathrm{m0}}(t) > 0' \end{cases} \tag{2.3}$$

where V_{damp} is amplitude of the damping voltage, $v_{\mathrm{transducer}}(t)$ is transducer voltage, and $i_{\mathrm{m0}}(t)$ is transducer motional current. Of course, such implementation would fail due to its quantized nature. The (2.3) allows transducer voltage to have only two values; nonetheless, it is a great starting point for exploration of nonlinear damping. At this moment let's assume there is a method how to modulate the voltage V_{damp}, such that damping can reach an arbitrarily low transducer voltage level.

To implement a system that could follow condition (2.3) it is necessary to have means to estimate motional current zero-crossing and align the transducer voltage to this information. This was in details described in [15]. The key idea is indicated by hardware in Fig. 2.1 and Fig. 2.2.

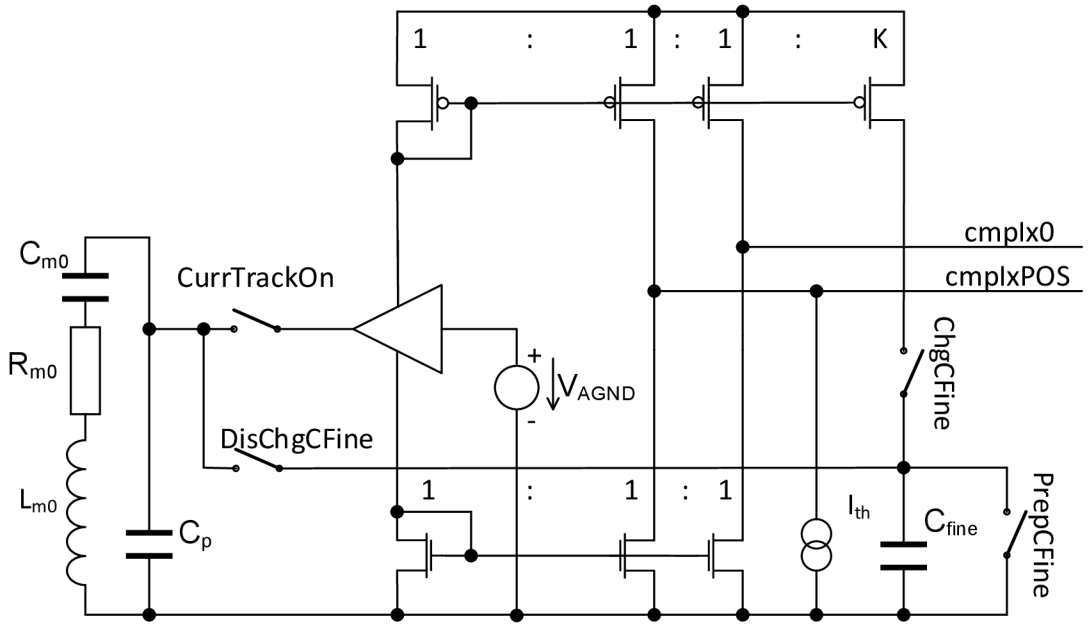

Fig. 2.1 Nonlinear fine damping circuitry [15]

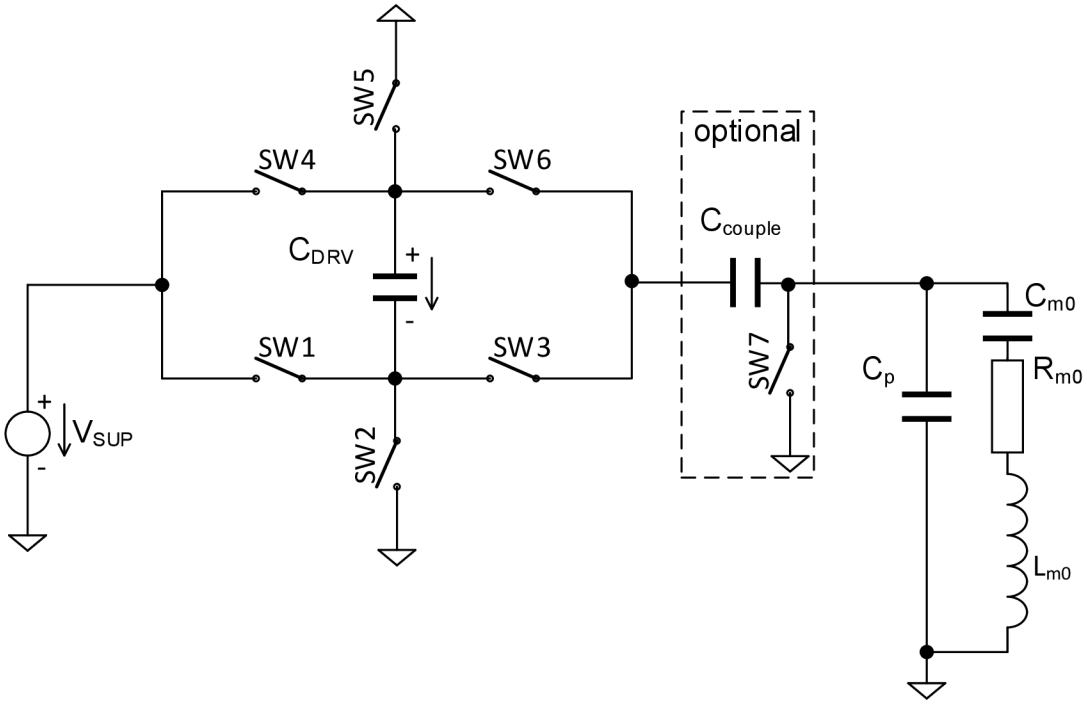

Fig. 2.2 Driver for transformer-less ULS with coarse nonlinear damping capability [15]

Fig. 2.1 shows the circuity for estimation of motional current zero crossings. To do this circuit must first estimate motional current. The hardware achieves this with buffer that forces voltage VAGND to the transducer. At the same time current through the buffer output stage is equal to transducer current and thus can be used for current monitoring. This is indicated by current mirrors that copy the buffer current to their output. Conveniently, the mirror outputs are also used to form current comparators.

There are two comparators forming output signals cmpIx0 and cmpIxPOS. Output cmpIx0 corresponds to current zero crossings. Output cmpIxPOS allows simple measurement of amplitude, by comparison with threshold current Ith, which enables the modulation of V_{damp}. In [15], system with fixed V_{damp} voltage was refered to as coarse nonlinear damping and system with variable V_{damp} was refered to as fine nonlinear damping. Simulation of system that implements coarse damping at the begining of reverberation followed by fine damping is shown in Fig. 2.3.

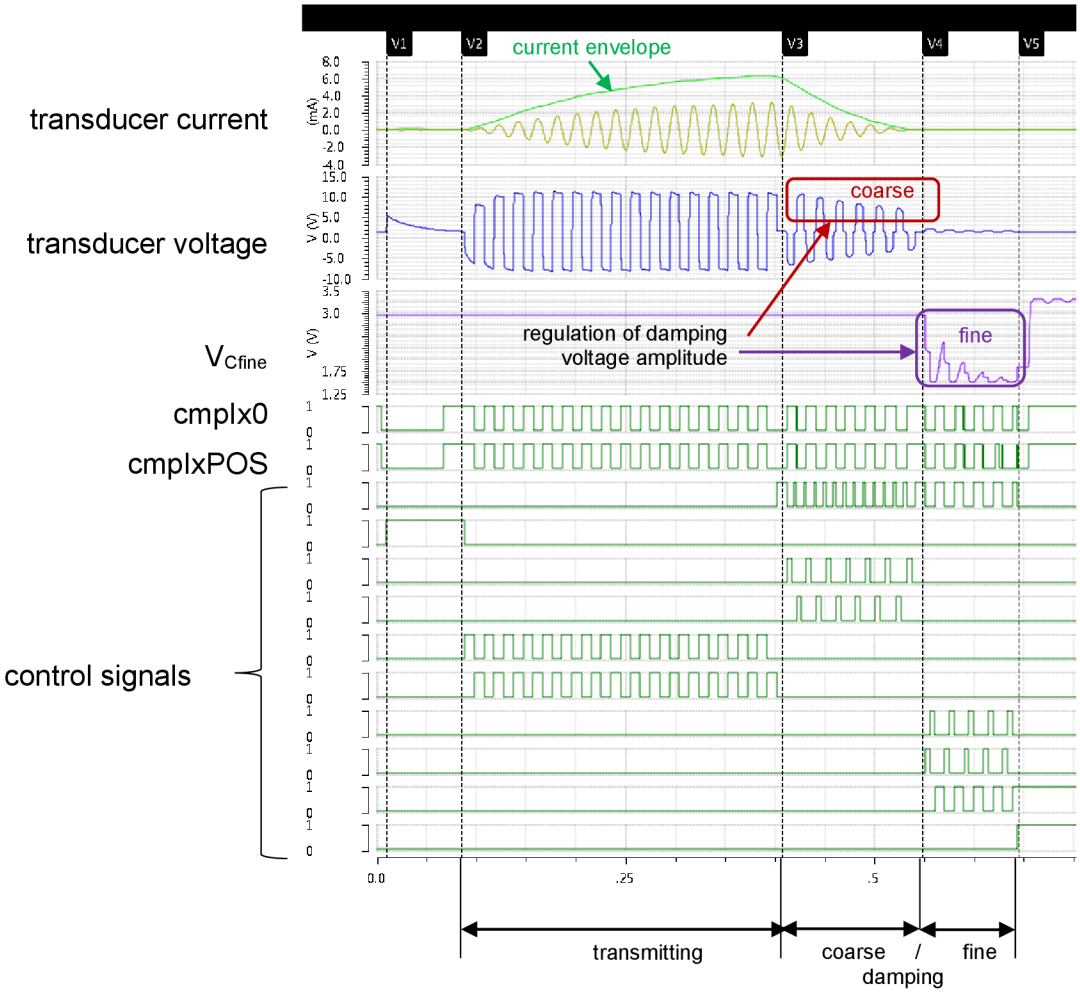

Fig. 2.3 Nonlinear damping simulation using single mode BVD model

2.2.1 Limitation of Nonlinear Damping due to Parasitic Resonances

Previous simulation results were obtain using a single mode BVD model, which does not represent broadband characteristics of transducer. Thus, a multimode transducer model was prepared. Model was created by manually tuning parameters to fit measured impedance characteristic of one selected transducer. Fig. 2.4 shows the measured impedance characteristic.

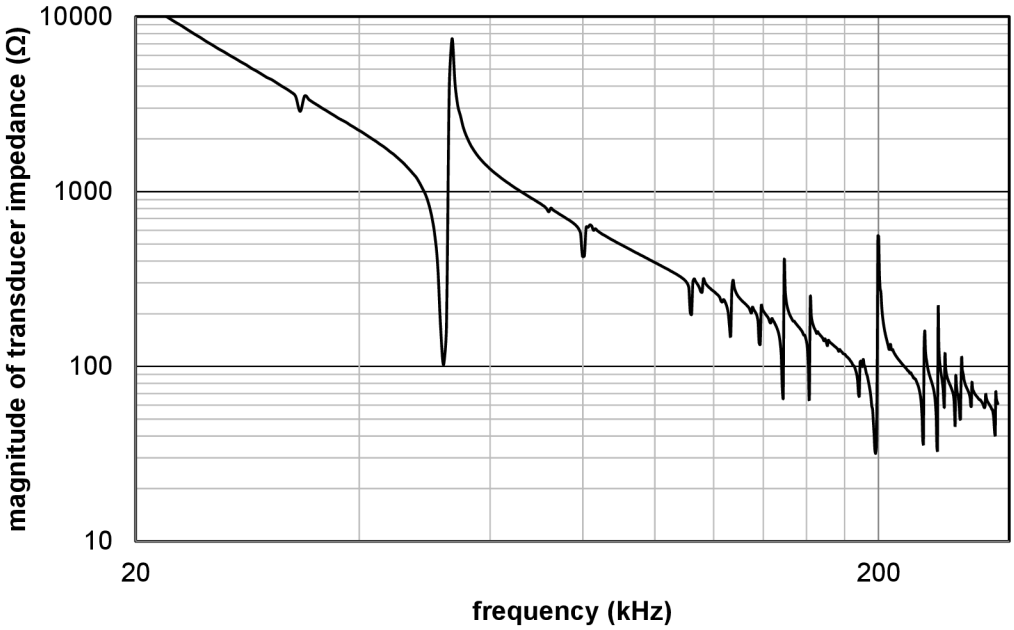

Fig. 2.4 Transducer impedance characteristic measured for purposes of evaluation of nonlinear damping

Afterwards the model was plugged into the simulation. The first result indicated problem in the circuitry for monitoring of motional current zero crossings. The circuitry started to produce incorrect timing information, which mislead system to produce incorrect damping pulses. The problem was apparent mainly at low amplitudes. This meant that coarse damping worked still well, but fine damping exhibited problems. Example of simulation result showing detail of transducer motional current, and comparator zero crossing is depicted in Fig. 2.5.

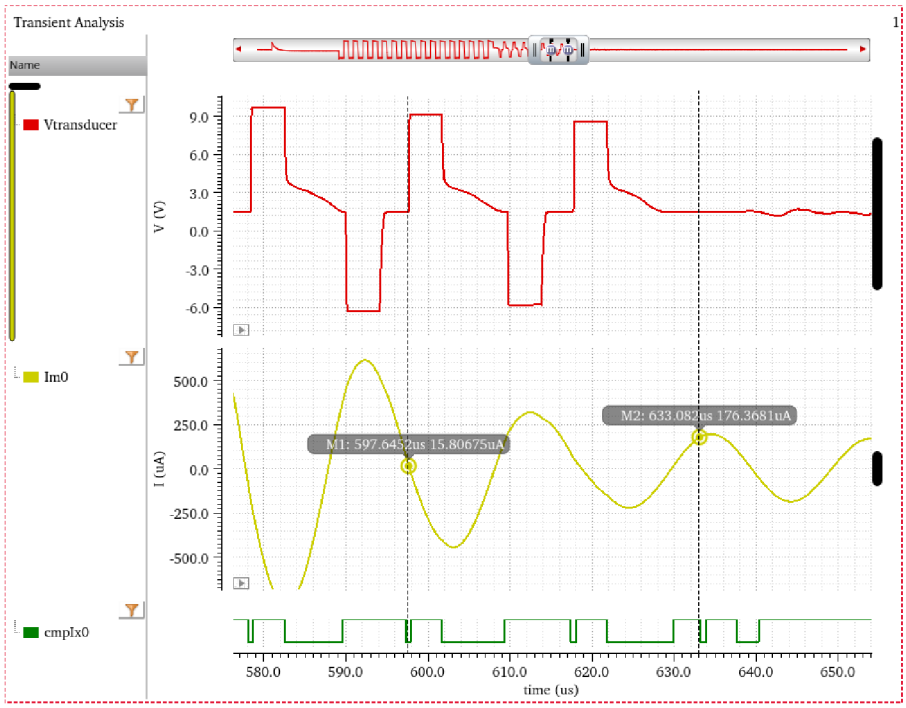

Fig. 2.5 Simulation result showing problem with zero crossing comparator (marker M1 shows correct response, and marker M2 shows false comparator trigger)

To confirm these findings a nonlinear damping evaluation platform was designed according to simulation schematic [16]. The board consists of standard receiver, distance measurement circuit, power supply, two transformer-less drivers suitable for coarse nonlinear damping, and circuit suitable for fine nonlinear damping. Fig. 2.6 shows photo of main board including attached transducer.

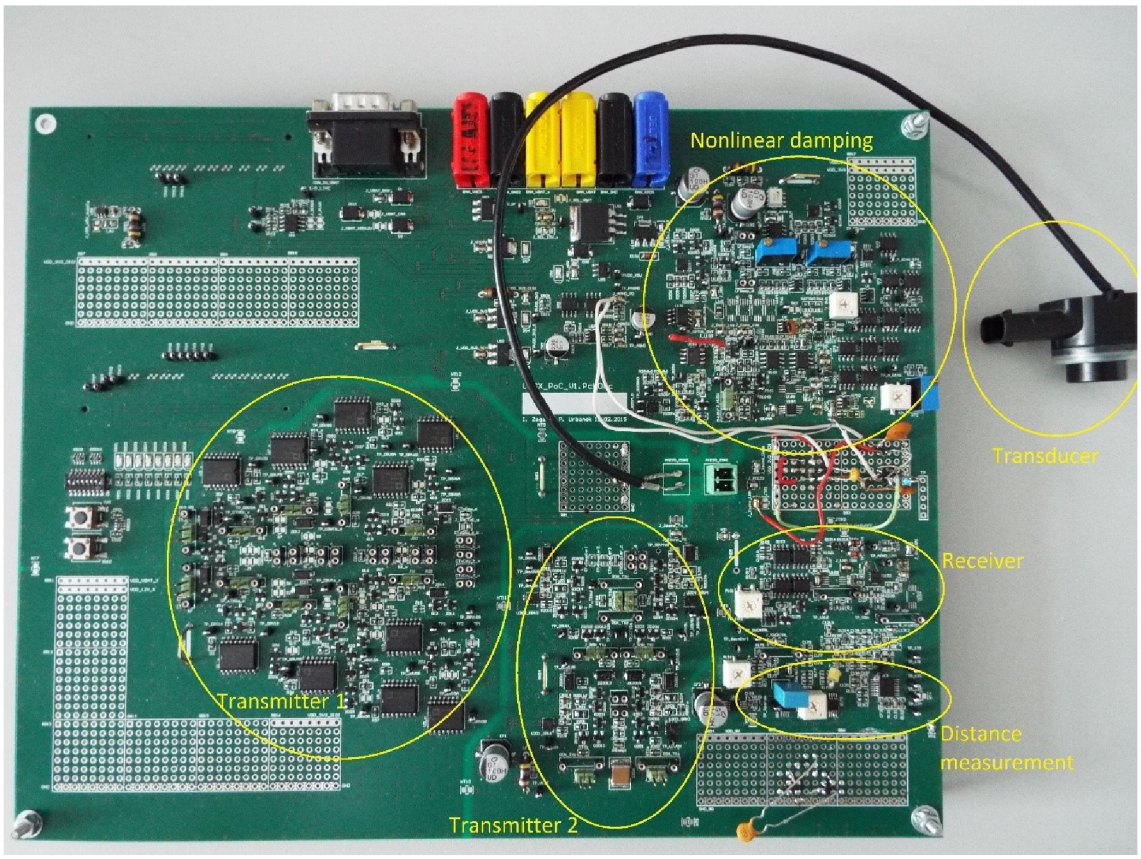

Fig. 2.6 Photo of nonlinear damping evaluation platform main board (taken from [16])

After standard functions such as receiving and transmitting were evaluated and verified, practical experiments with nonlinear damping could be carried out. First experiment aimed to embed both coarse and fine nonlinear damping. As predicted by simulation the coarse damping worked well, and fine damping exhibit problems. In many cases system failed to stop fine damping, and instead start to oscillate on some parasitic frequency. Example of such a behavior is in Fig. 2.7. The figure shows last coarse damping cycle followed by fine damping with lowered gain, during which parasitic resonance is excited.

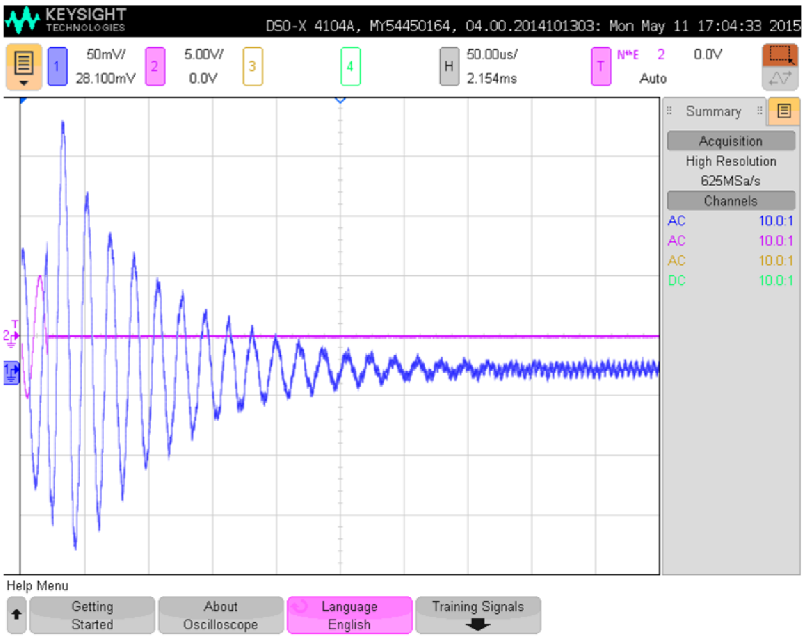

Fig. 2.7 Oscilloscope snapshot showing oscillation of fine nonlinear damping system on parasitic frequency

2.3 Linear Damping

The previous part of this chapter focused solely on nonlinear damping circuits. Although, the nonlinear damping methods are attractive at the beginning of damping phase, in later stage the problem with excitation of parasitic resonances means the damping fails. Consequently, we are left with a linear damping circuits. The ideal linear damping circuit would be a negative capacitance, however, its low robustness and susceptibility to unstable operation is killing factor for automotive design. Alternatively, one can focus on LR parallel shunt, as depicted in Fig. 2.8. It is the same type as is used in current ULS with the transformer.

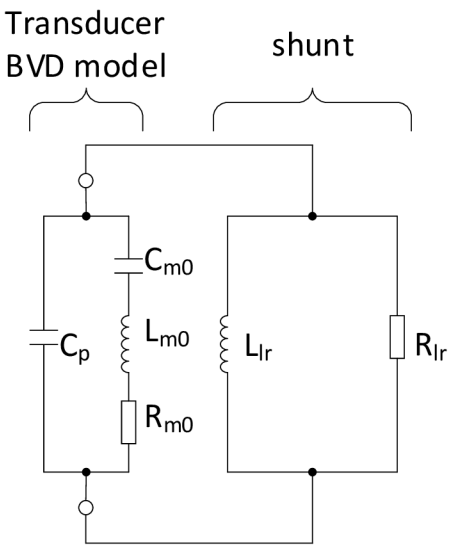

Fig. 2.8 Equivalent networks showing single mode BVD model with inductive/resistive parallel shunt

Assuming the transducer's motional resistance R_{m0} is negligible, it can be shown that ideal damping condition is given by equations

$$L_{lr} = \frac{C_{m0} L_{m0}}{C_p}, \tag{2.4}$$

$$R_{lr} = \frac{1}{2}\sqrt{\frac{L_{m0}}{C_p}}, \tag{2.5}$$

where L_{lr} is ideal value of shunt inductance, R_{lr} is ideal value of shunt resistance, L_{m0}, C_{m0}, and C_p are transducer parameters. The condition (2.4) is derived from equivalence of parallel and serial resonance frequency. Similarly, equation (2.5) is derived from equivalence of Q-factors.

The Fig. 2.9 shows how reverberation time varies with shunt setting for a given transducer. We can clearly see there is optimum setting that corresponds to equations (2.4) and (2.5). Obviously, it is desirable to have a method how to find such a setting. This was addressed in [17], and is briefly described in coming paragraphs.

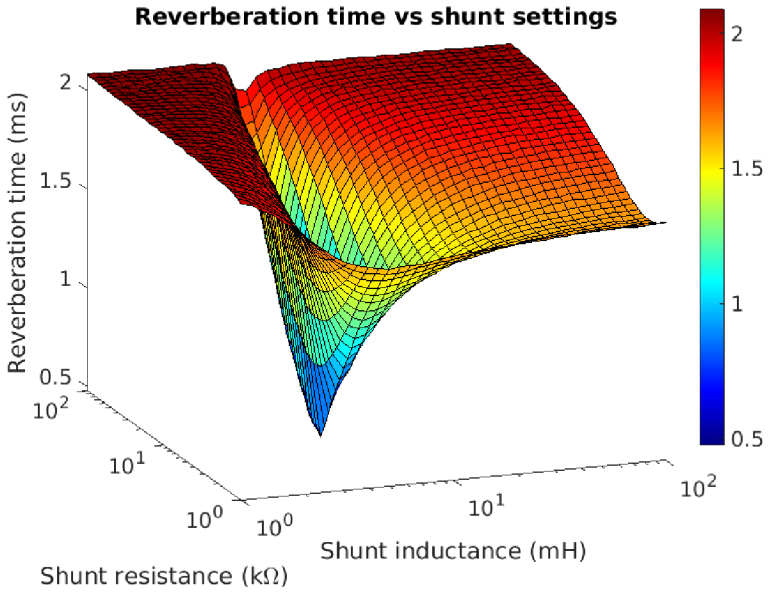

Fig. 2.9 Damping performance as function of LR shunt parameters

2.3.1 Adaptive Tuning of LR Shunt

Suppose we can arbitrarily control inductance and resistance of connected shunt, furthermore, we can also fully disconnect either inductance or resistance element of shunt circuit. Let us suppose the shunt has inductance of L_{pw}, which is not the ideal shunt value. The ideal shunt value is L_{pc} and is unknown to the system. The inductance can be scaled up by a factor of K_{scale} to allow measurement of parallel resonant tank only. The transducer resonance frequency can be also measured when shunt is disconnected. We also know, that condition (2.4) was derived from the assumption of resonant frequency equivalence. This means that inductance of L_{pw} results in resonant frequency mismatch, and inductance of L_{pc} results in matching resonant frequencies. To tune the shunt system must do following:

- Measure transducer main motional frequency
- Measure parallel resonance frequency (using inductance scaling)
- From frequency mismatch predict correction factor, and adjust inductance
- Periodically repeat these steps to ensure continuous tracking of ideal damping

Assuming we have successfully, tuned inductive part of the shunt we can continue to resistance tuning. The ideal shunt resistance is derived from equivalence of Q-factors. However, derivation process also stumps upon interesting relation, which one can rewrite into

$$R_{\mathrm{lr}} = \frac{1}{2}\sqrt{Z_{0\mathrm{p}} Z_{0\mathrm{s}}}. \tag{2.6}$$

This shows that ideal damping resistance is proportional to geometrical average of characteristic impedances of two resonant tanks. Now we need the assumption of

previously tuned inductance part of the shunt. The fact, that inductance is tuned means that the system knows also characteristic impedance of parallel tank $Z_{0\mathrm{p}}$, since it knows inductance and resonant frequency. The challenge is in obtaining characteristic impedance of transducer $Z_{0\mathrm{s}}$. The suggested idea is to measure motional resistance of transducer R_{m0} and transducer Q-factor. Using these two parameters one can express characteristic impedance of transducer and all inputs are available for the system. The concept for resistance tuning is then following:

- Measure transducer characteristic impedance through motional resistance and Q-factor measurement
- Calculate/measure characteristic impedance of parallel tank (from tuned shunt inductance and resonant frequency)
- Predict ideal shunt resistance, and adjust shunt resistance
- Periodically repeat these steps to ensure continuous tracking of ideal damping

At this moment one has means to implement predictive tuning system capable of adjusting both shunt inductance and resistance.

3 IMPLEMENTATION OF LR SHUNT SUITABLE FOR ADAPTIVE TUNING

The preferred linear shunt circuit for ULS transducer is parallel combination of inductor and resistor. It is mainly due to inherent stability (robustness) and simplicity. To realize the inductance Grounded Inductor Simulator (GIS) is employed. Although many different GIS topologies exist in literature, to author´s best knowledge, none of them is able to meet requirement for the transformer-less damping applications and more specifically aspects concerning shunt tuning capabilities. As a result, author in [18] presented a novel GIS topology. The topology origins from Ford-Girling gyrator [19] with two modifications; input voltage buffer, and output current buffer. Another important feature of newly proposed GIS relates to wide control range of its inductance, which will be described in detail shortly.

The Fig. 3.1 shows original Ford-Girling topology and newly proposed one. The buffers in proposed topology allows power switches to be part of the feedback, which makes it immune to switch resistance. We should also acknowledge the fact that proposed topology does not require amplifier with gain of 2, which limits dynamic range of original Ford-Girling structure.

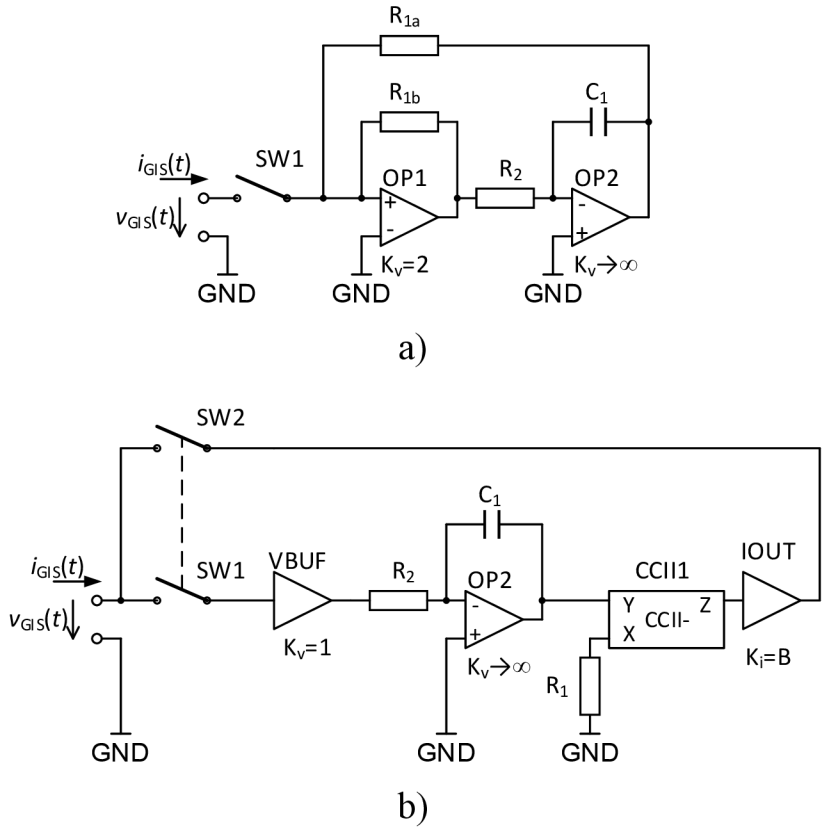

Fig. 3.1: a) Ford-Girling GIS structure b) proposed GIS structure

3.1 GIS Custom Control Scheme

Practical realization of large inductance range with high resolution is one of the main aspects that underlines the whole circuit topology. A range from 0.8 mH to 100 mH would be needed to cover the temperature operating range, process variations in ASIC and transducer, plus needs of the adaptive tuning algorithm. Furthermore, the resolution would have to be 10 μH. These are very challenging parameters.

In real application, however, inductance control can be split to multiple functions. To address manufacturing variation, there could be trimming function. Another function realizes inductance scaling by factor of K_{scale}. And remaining function is for inductance tuning itself. However, once the shunt is tuned, there is no reason to change the inductance significantly. In fact, the inductance must change only to track variation in temperature or other environmental aspects. In general, one can assume that these changes will be rather slow. Therefore, it makes sense to split the inductance control even more. As an educated guess the *tuning* input was split into *tuning_coarse_code* and *tuning_fine_code* inputs. This means achieving monotonicity of these function will be much easier, which is crucial for tunning itself. Nonetheless, the monotonicity applies only to individual functions. When both control functions are employed, resulting control scheme is not required to guarantee monotonicity. Meaning, if the two inputs *tune_coarse_code* and *tune_fine_code* are merged into a single input *tune_merge_code*=[*tune_coarse_code*, *tune_fine_code*] there does not have to be any ordering rule for *tune_merge_code* to form monotonous transfer function. In another words, if we use pairs of *tune_coarse_code* and *tune_fine_code* as x-axis values to form a graph and GIS inductance is on y-axis the result does not have to be monotonous, no matter what sort of ordering is used on x-axis. The complete tuning function is depicted in Fig. 3.3. The detail of two adjacent coarse codes is depicted in Fig. 3.2.

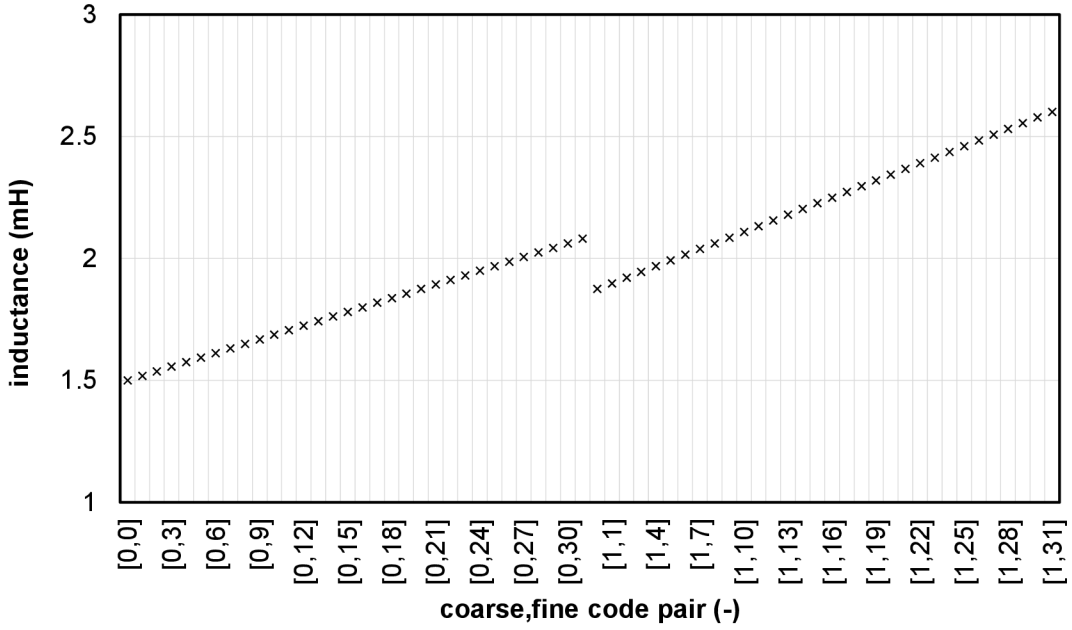

Fig. 3.2: Overlap of adjacent coarse ranges

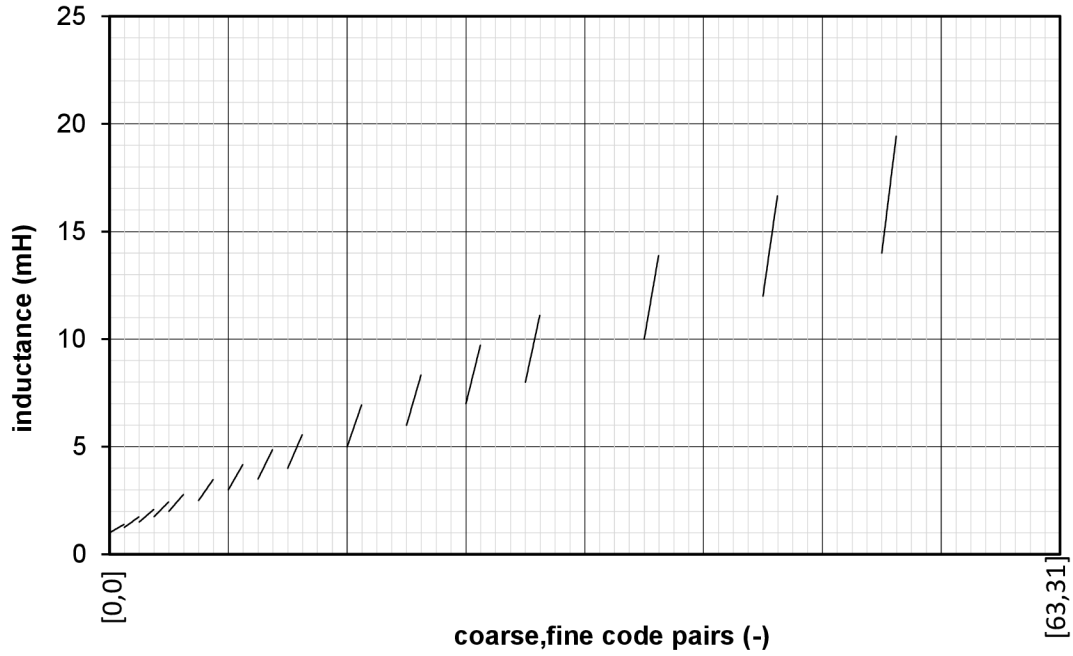

Fig. 3.3: Inductance control for exponential coarse control

3.2 GIS Verification Results

Last step in GIS implementation was verification of a complete GIS circuitry. The verification consists of full top level simulations and practical measurements of manufactured GIS. Results from measurements and simulations are compared to make sure everything aligns as expected. The GIS design was manufactured in I4T

technology. This technology features 0.18 µm CMOS with high voltage extension. The GIS chip photo is shown in Fig. 3.4.

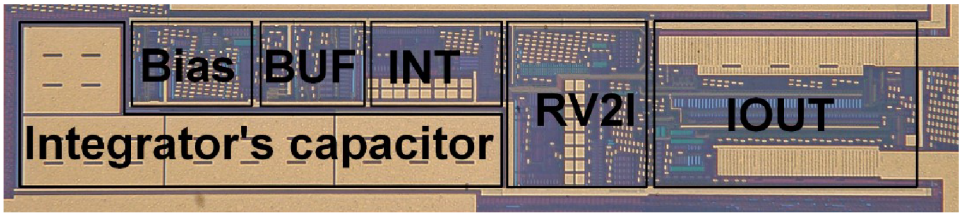

Fig. 3.4: Photograph of GIS circuitry (taken from [18])

To confirm GIS suitability for adaptive tuning, its control characteristics were measured and evaluated for linearity. In Fig. 3.5 there is control characteristic of *tune_coarse_code* and corresponding DNL and INL is evaluated. Similarly, Fig. 3.6 shows control characteristic of *tune_fine_code* and corresponding DNL and INL. It is important to note, that results in Fig. 3.6 were obtain in measurement with opened GIS loop, which enabled higher resolution necessary for DNL and INL evaluation. This is in contrast with result presented in [20], in which inductance was measured with closed GIS loop. This led to worse DNL and INL result, although it was still within the expected boundary of 1 LSB.

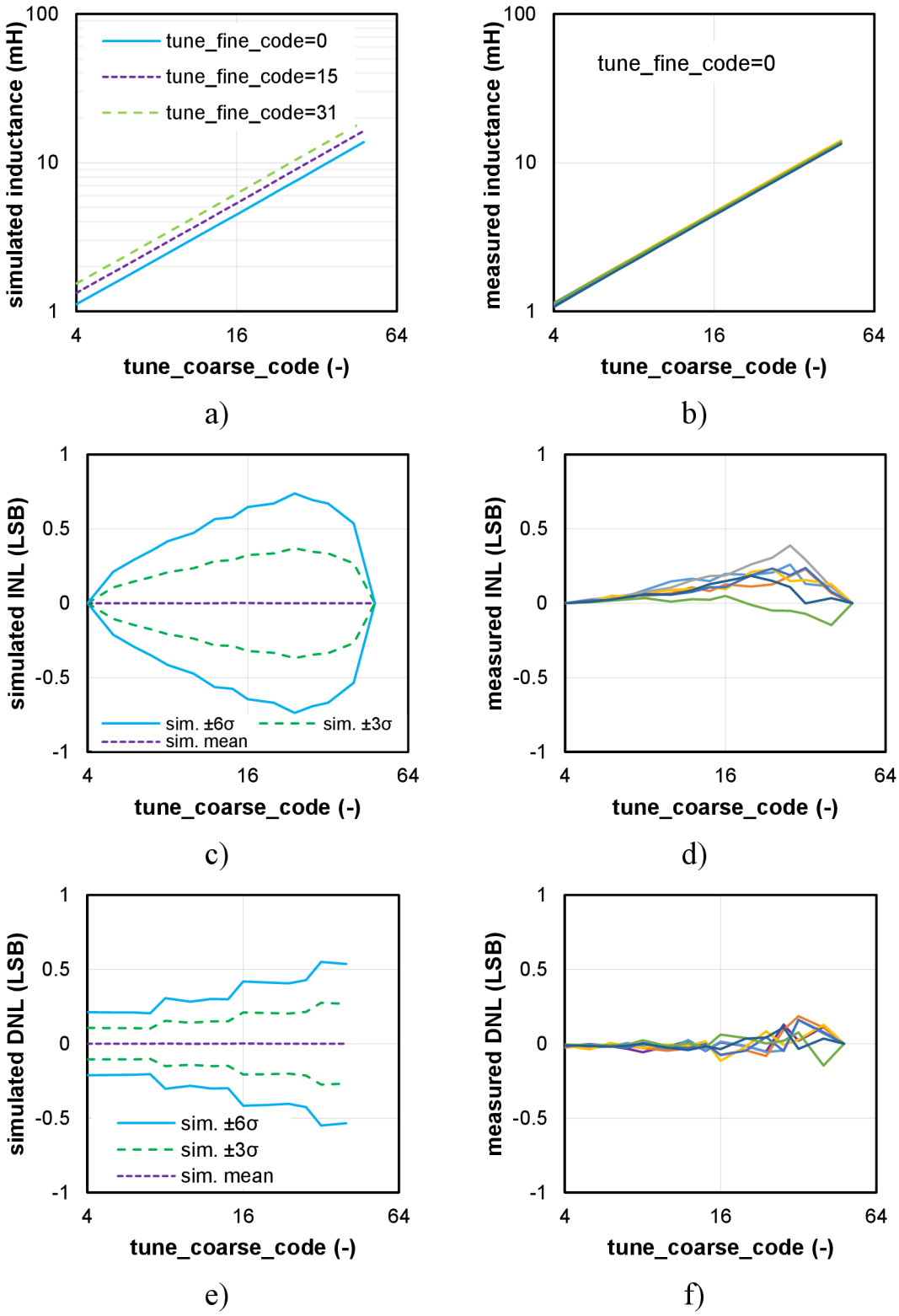

Fig. 3.5: GIS coarse control function a) simulated, b) measured. INL of control function c) simulated, d) measured. DNL of control function e) simulated, f) measured.

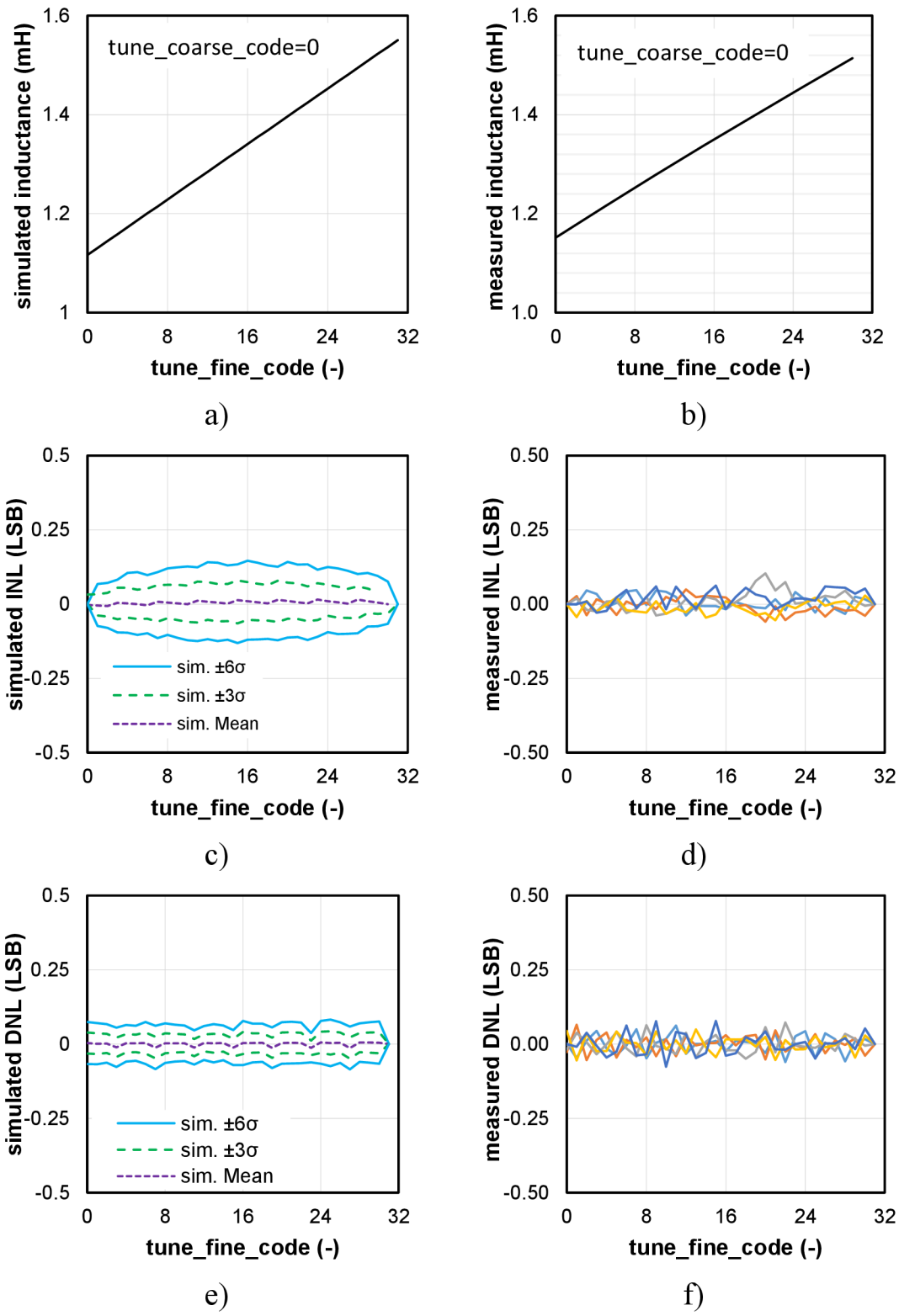

Fig. 3.6: GIS fine control function a) simulated, b) measured. INL of control function c) simulated, d) measured. DNL of control function e) simulated, f) measured. (due to the measurement setup limitations, the GIS inductance was measured with opened loop)

Another important GIS parameter is its Q-factor. The Q-factor determines GIS losses, which should be relatively small otherwise, the ring-down measurement methods utilizing the GIS may fail. The Fig. 3.7 shows measured and simulated Q-factor as function of GIS inductance. The plot shows nominal inductance and its scaled up variant. We can see that GIS struggles to maintain Q-factor above 10 for high inductance values. Based on preliminary simulation of complete system, the expectation for Q-factor was to be always above 10, and for perfect performance the Q-factor should be above 30. Here, we see certain marginality in GIS performance, however, for most of the available transducers the GIS performance is sufficient.

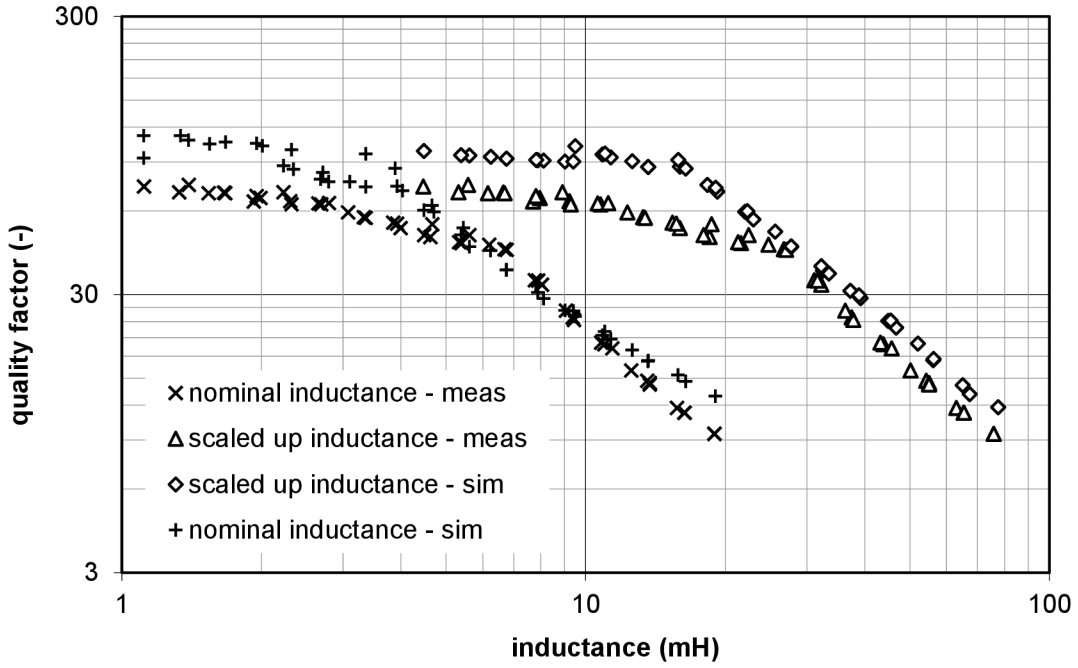

Fig. 3.7: Measured and simulated Q-factor versus inductance

Last important verification step focuses on GIS dynamic range. THD and noise floor define this range. The THD simulation and measurement results are summarized in Fig. 3.8. Both simulation and measurement agree, showing a knee around 0.9 – 1.0 V_{rms}. This well matches with the design expectation, since the limiting factor is voltage swing on GIS output, which is reaching the supply levels. Noise was measured as effective noise voltage in bandwidth of interest. The measurement used chip internal signal processing circuitry to evaluate complete chain including the GIS. The GIS noise floor was expected to be dominant, thus the result can be considered almost equal to the GIS intrinsic noise. The estimated voltage noise is 200 μV. The simulation of integrated noise resulted in 230 μV.

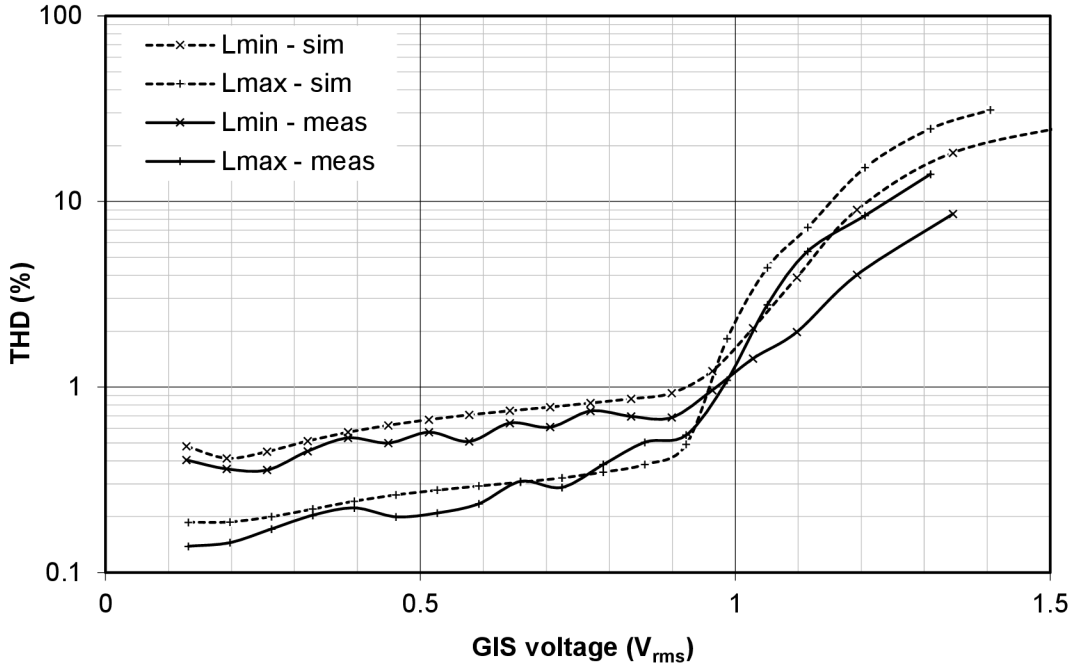

Fig. 3.8: Measurement and simulation of THD

To conclude this chapter, complete overview of key GIS parameters is shown in Table 3.1.

Table 3.1 Overview of achieved GIS parameters

Parameter	Required	Simulated	Measured	units
frequency range	44 – 69	40 – 75	-	kHz
basic inductance range	1.22 – 17	1.12 – 18.9	-	mH
Q-factor	>10	11.8	11.2	-
THD①	<1	0.92	0.71	%
tuning step	<1	0.91 – 1.26	-	%
tuning linearity (INL, DNL)	<1	0.75	0.38	LSB
area	<1	-	0.216	mm^2
noise floor	<500	230	200	uV_{rms}
dynamic range	>66	71.8	73.1	dB

① at 0.9 V_{rms}

4 REALIZATION OF ADAPTIVE DAMPING CONCEPT UTILIZING NONLINEAR DAMPING AND TUNING OF LR SHUNT USING INDUCTANCE SCALING

Number of different damping concepts were reviewed in the thesis. As most suitable combination for transformer-less ULS in PAS, coarse nonlinear damping followed by an adaptive LR shunt damping was suggested. This chapter focuses on practical realization of such a system including its verification as a complete concept.

As indicated in Fig. 2.9, reverberation performance is more sensitive to proper setting of inductance. Furthermore, the ideal damping setting versus temperature shows much higher variation in case of inductance, as is documented by Fig. 4.1.

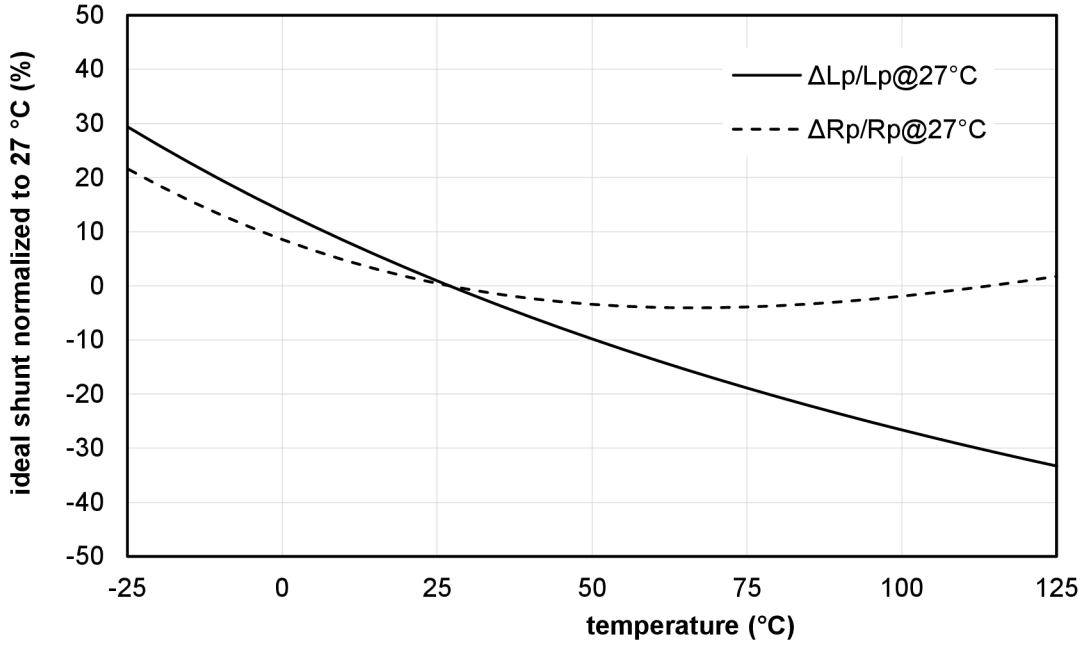

Fig. 4.1: Ideal LR shunt parameters versus temperature (taken from [20])

Considering lower sensitivity to ideal damping resistance and also lower temperature variation in ideal damping resistance, one can implement a simple one point calibration (manufacturing trimming) of this parameter. The simulation in Fig. 4.2, shows result of damping performance with ideal damping resistance, and with 20% error in resistance. We see that in vicinity of ideal shunt setting the damping resistance error limits our performance, however, the impact is not that severe, considering that 20% is the worst case variation taken from Fig. 4.1. This justifies the proposed idea of non-adaptive resistive part of shunt circuit. Practical implementation of such a solution requires only Non-Volatile Memory (NVM) that is typically present in every automotive ASIC and trimming during the manufacturing of complete ULS.

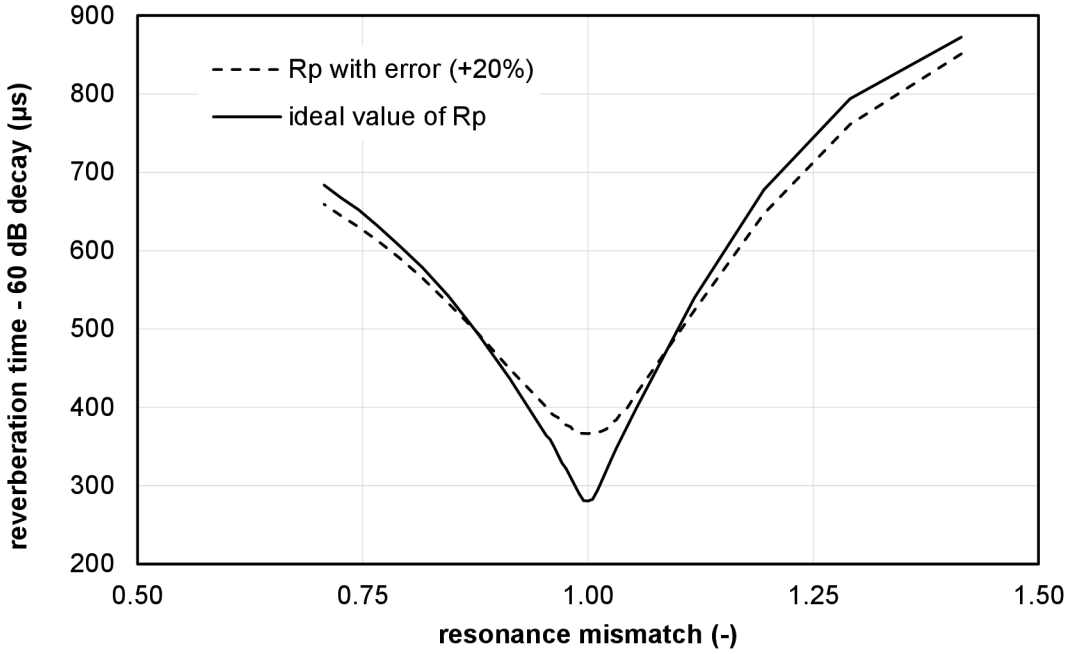

Fig. 4.2: Simulated impact of inductance tuning curve for ideal damping resistance, and damping resistance offset by 20% (taken from [20])

4.1 Nonlinear Coarse Damping

As described in chapters 2.2, the nonlinear coarse damping hardware consists of modified driver and zero crossing current comparator. For practical on chip realization the modified driver proposed in Fig. 2.2 was used. This driver requires external capacitor C_{drv}, but the capacitor allows doubling of driving/damping voltages, which is highly appreciated in transformer-less application. The switch design supports operation with supply from 10 V up to 40 V, and for flexibility switch control can be external to the IC.

4.2 Predictive Inductor Tuning Method

Chapter 2.3.1 mentioned the condition of ideal damping. The shunt parameters must be set such that resulting resonant circuits will have same characteristic parameters (resonant frequency and Q-factor). Ideal shunt inductance value leads to perfectly matched resonant frequencies.

If the two resonances do not match (f_{m0} is not the same as f_p), because shunt inductance L_{pw} is set incorrectly, the wrong parallel resonance frequency f_{pw} can be expressed as

$$f_{pw} = \frac{1}{2\pi\sqrt{L_{pw}C_p}}. \tag{4.1}$$

The resonances mismatch M_{res} can be expressed as

$$M_{\text{res}} = \frac{f_{\text{m0}}}{f_{\text{pw}}}. \tag{4.2}$$

On the other hand, desired situation when the resonances do match means inductance has correct value of L_{pc}, which corresponds to the correct parallel resonant frequency of f_{pc}. We can describe the situation as

$$f_{\text{pc}} = \frac{1}{2\pi\sqrt{L_{\text{pc}}C_{\text{p}}}}. \tag{4.3}$$

Combining (4.1), (4.2), and (4.3) will yield

$$L_{\text{pc}} = \frac{1}{M_{res}^2} L_{\text{pw}} . \tag{4.4}$$

If we know the resonant frequencies mismatch it is possible to correct the wrong shunt inductance L_{pw} by changing it by the factor of $\frac{1}{M^2}$. To enable measurement of fpw inductance scaling is needed to avoid interference of f_{pw} and f_{m0}. Consequently, equation (4.1) can be rewritten to

$$f_{\text{pw}} = \frac{1}{2\pi\sqrt{K_{\text{scale}}L_{\text{pw}}C_{\text{p}}}} . \tag{4.5}$$

And equation (4.2) changes to

$$M = \frac{f_{\text{m0}}}{\sqrt{K_{\text{scale}}}f_{\text{pw}}} . \tag{4.6}$$

Knowing K_{scale} is 4, and having measured f_{pw}, and f_{m0}, system can calculate mismatch of resonances according to (4.6). From this mismatch system can predict correcting factor and change shunt inductance value from L_{pw} (by factor of $\frac{1}{M^2}$) to L_{pc}. At this point we can expect ideal shunt value is achieved. However, careful reader will remember that shunt inductance hardware implementation has two tuning inputs. Consequently, the tuning must be done at least in two steps. In first step, *tune_coarse_code_wrong* is adjusted to *tune_coarse_code_correct* followed by a second step, which adjusts *tune_fine_code_wrong* to a value of *tune_fine_code_correct*. This adjustment can be described by (4.7), and (4.8).

$$tune\_coarse\_code\_correct = \frac{tune\_coarse\_code\_wrong}{M^2}. \quad (4.7)$$

$$tune\_fine\_code\_correct = \frac{80+tune\_fine\_code\_wrong}{M^2} - 80. \quad (4.8)$$

4.3 Experimental Hardware and Measurement Results

To verify performance of a complete transformer-less ULS, dedicated analog test chip was manufactured in onsemi's I4T technology (180 nm CMOS with high voltage capability). The test chip contains transducer driver capable of nonlinear damping, a digitally controlled synthetic inductor described in chapter 3, receiver, and additional support circuitry including serial control interface. To support the testchip a prototyping platform was prepared [21]. The test chip and prototyping platform for evaluation is depicted in Fig. 4.3.

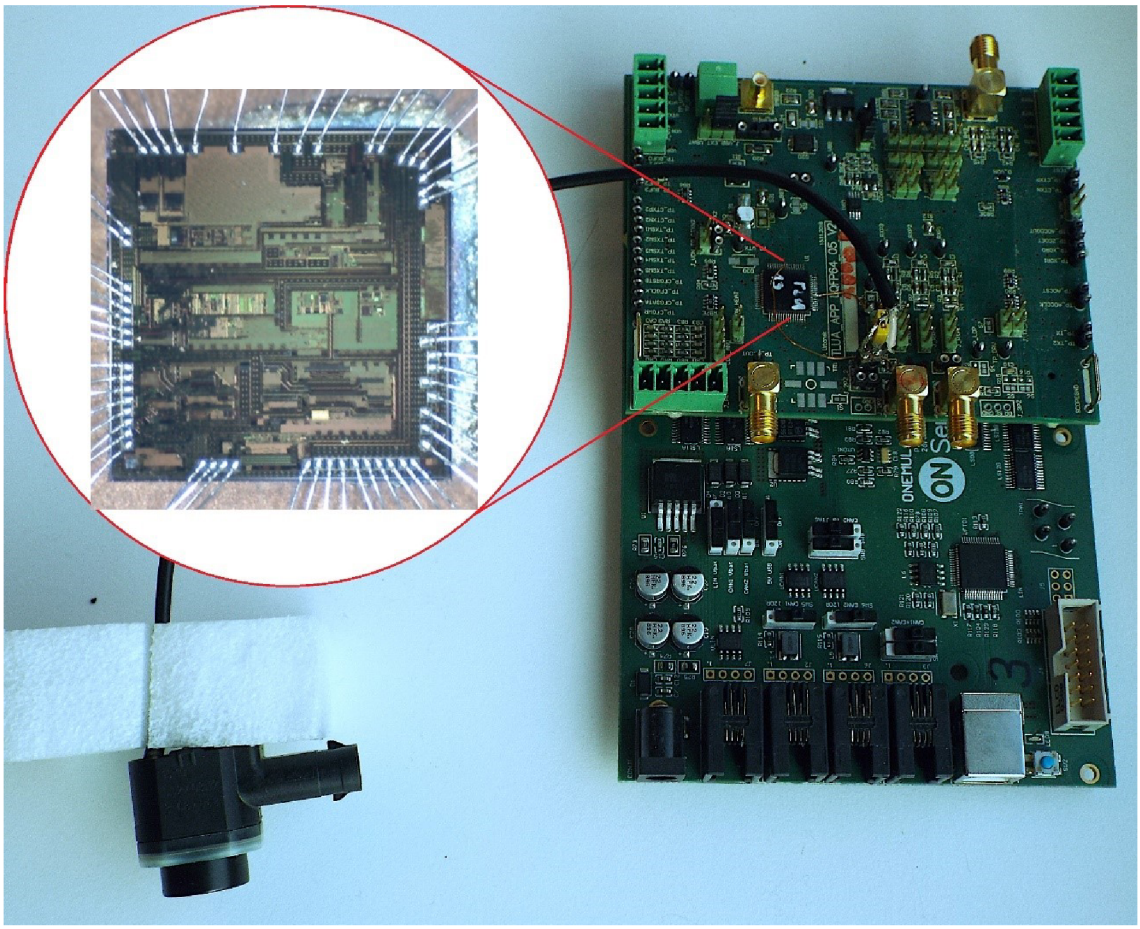

Fig. 4.3 Prototyping hardware platform including the test-chip (taken from [20])

4.3.1 Verification of Inductance Tuning

For verification of inductance tuning the nonlinear damping is disabled. This is to avoid unwanted interaction between the damping systems. In addition, the shunt resistance is manually set to mimic manufacturing trimming.

To demonstrate correct shunt tuning capability the shunt inductance was manually swept in its full range and reverberation time was measured, resulting dependency is in Fig. 4.4 where it is compared with a setting that was found by the implemented algorithm. The found optimum differs by less than 2%.

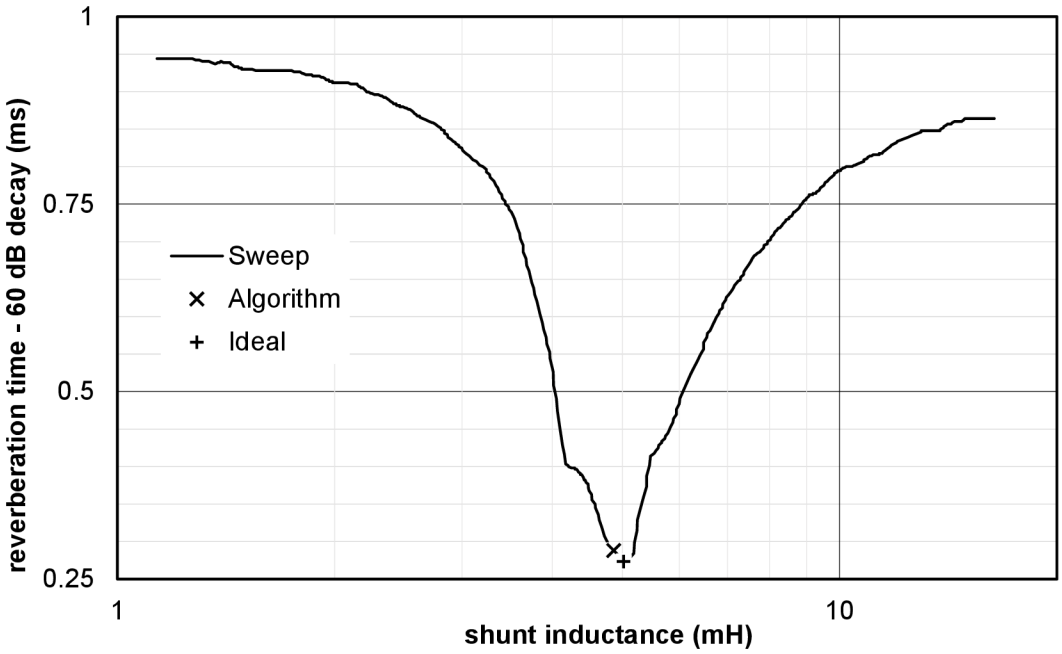

Fig. 4.4 Tuning setting found by proposed algorithm versus the ideal optimum obtain from manual sweep (taken from [20])

In Fig. 4.5 it is depicted how the inductance value changes during application run after each distance measurement cycle. Both ideal and calculated inductance are shown for comparison. The ideal inductance was found using manual sweep. Cycle 0 is not depicted, but it corresponds to an initial condition, which was intentionally set to 17 mH. To demonstrate algorithm adaptability to sudden changes, a 1 nF capacitor is connected in parallel to the transducer between cycles 10 and 11, and similarly the capacitor is disconnected between cycles 20 and 21, thus significantly changing circuit properties. The value calculated by the algorithm can quickly track these changes. For better comparison Fig. 4.5 also shows corresponding difference between ideal and calculated value.

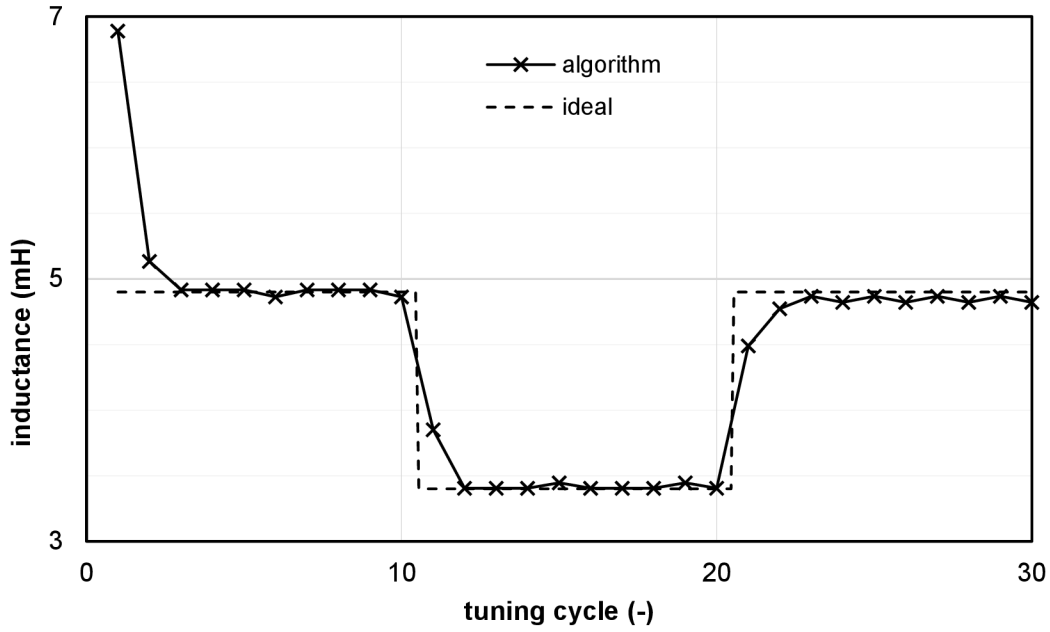

a)

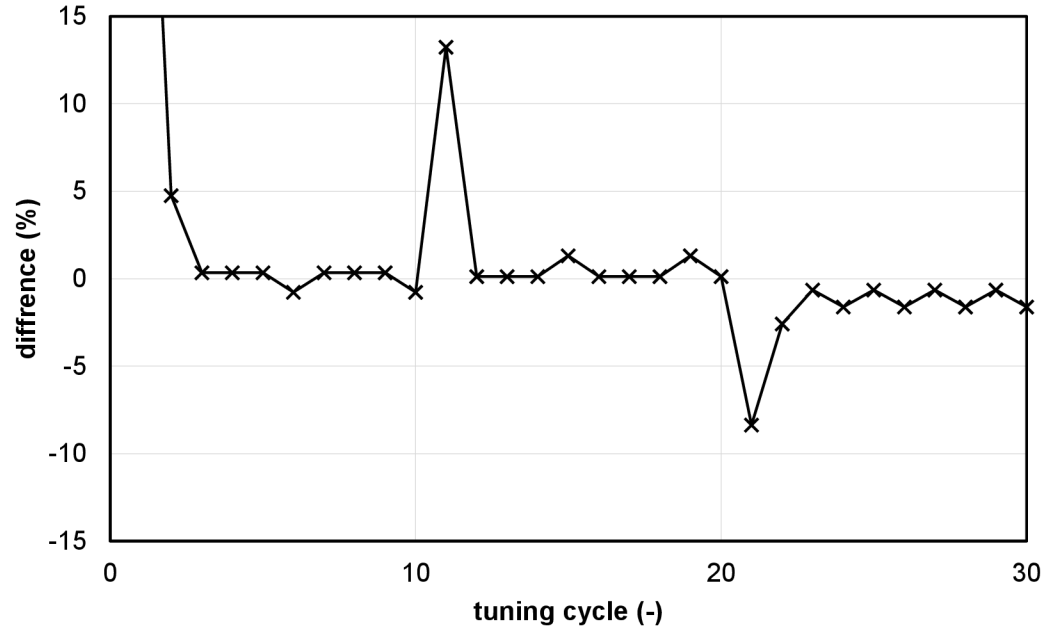

b)

Fig. 4.5 a) shunt inductance setting versus consecutive distance measurement cycles and b) corresponding difference (after 10th and 20th cycle additional parallel capacitor was connected/disconnected to the transducer) (taken from [20])

4.3.2 Measurement of Complete Assembly (Nonlinear Damping + Tuned Linear Damping)

To prove complete concept is viable, experiments on complete assembly of nonlinear and linear damping were performed. As described previously, the concept advocates use of modified transformer-less driver, which can also support nonlinear damping.

In addition, the system uses adaptive tuning of linear shunt. In Fig. 4.6 complete distance measurement cycle is depicted. Individual sub-phases are marked as Ph1 – Ph6. Ph1 is inductor tuning phase, Ph2 is preparing of TX driver (charging auxiliary capacitors), Ph3 is transmitting phase, Ph4 is nonlinear coarse damping, Ph5 is damping with shunt inductance, and Ph6 is distance measurement phase (depending on maximum distance, continues up to ~40 ms).

Compared to experiment in chapter 4.3.1, this chapter introduces nonlinear damping and focuses on evaluation of distance measurement rather than direct measurement of damping performance. The nonlinear damping presents certain challenge for evaluation. The amount of residual energy after nonlinear damping phase cannot be controlled, which means that damping time varies and similarly the residual energy. However, important observation is that by employing the nonlinear damping, system always improves overall performance. Typical saving in damping time is ~200 µs.

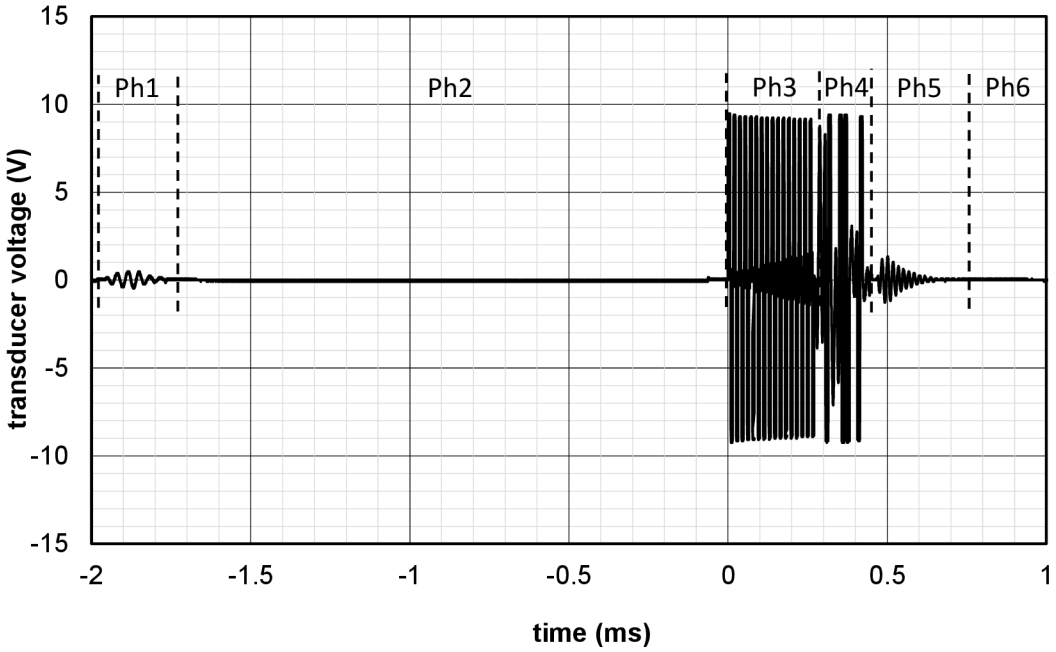

Fig. 4.6: Distance measurement cycle with indicated subphases

So, to evaluate adaptive capability of proposed system following experiment was performed. The system was trimmed at 27 °C for ideal damping resistance. Next the temperature was swept, and damping performance was measured with enabled adaptive tuning, with manually set ideal damping inductance and disabled adaptive tuning. Table 4.1 shows achieved minimum distance as function of temperature. The most important observation is that adaptive tuning performance is equal to manually set ideal damping. The data are also plotted in Fig. 4.7 to visualize how performance

changes with variation in temperature. The adaptive system shows very little variation compare to simple trimming at one temperature. We should note that temperature range for this experiment was limited to -20 °C – +80 °C due to limitations of some components on the development board. However, for the purpose of idea evaluation this temperature range is sufficient. Note, due to the way how echo detector is implemented the measurement is done with distance step of 1cm, which somewhat skews the results.

Table 4.1 Measured distance versus temperature for different scenarios

temperature (°C)	Minimal measured distance (cm)		
	shunt value trimmed at 27 °C	manually found ideal shunt setting	setting find by tuning algorithm
-20	21	19	19
27	18	18	18
50	20	18	18
80	21	18	18

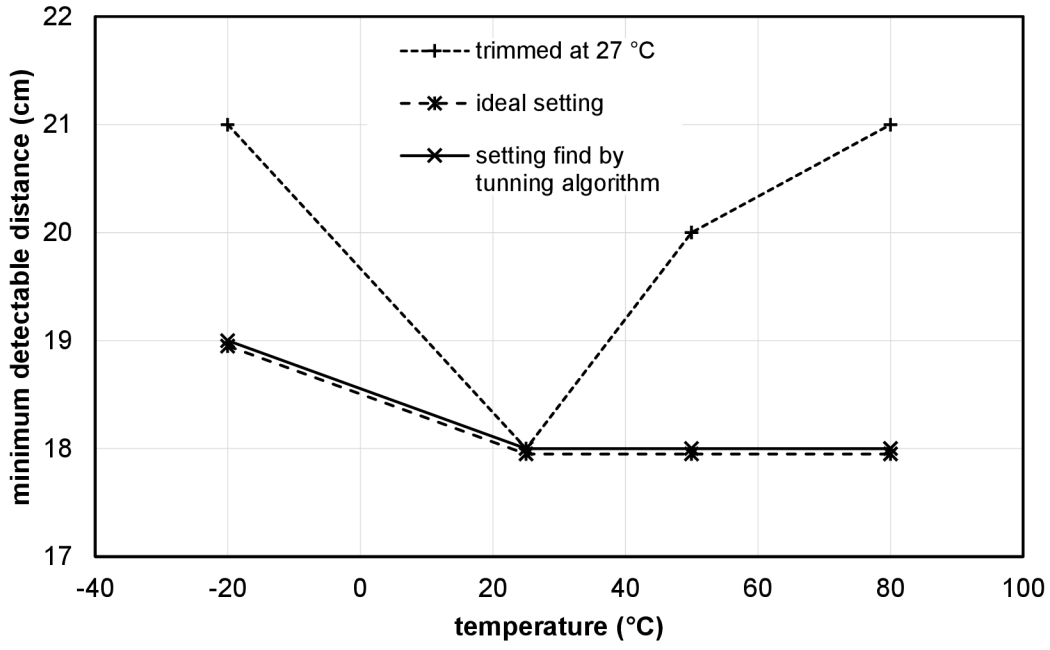

Fig. 4.7 Minimum detectable distance as function of temperature

5 CONCLUSIONS

This thesis focuses on advancement of Ultrasonic Sensors (ULS) used in Park Assist Systems (PAS). To achieve the main objective the thesis intentionally sets four intermediate goals, which are:

Goal 1: to develop a theoretical foundation for transducer damping and reverberation reduction,

Goal 2: to evaluate, develop, or verify transducer parameter measurement methods suitable for integration into an Integrated Circuit (IC),

Goal 3: to design a custom hardware for the proposed damping concepts and,

Goal 4: to verify performance of the complete transformer-less ULS concept.

Ad 1: The reverberation reduction is the key topic in the thesis. To tackle the problem, the theoretical foundations were investigated. Most important findings are in chapter 2. This activity resulted in two patent applications [15], [17]. The first patent focuses on nonlinear damping concepts. The patent was filled first, since initial expectations were that nonlinear systems would perform better [15]. The patent proposed a coarse and fine nonlinear damping, depending on control of damping voltage amplitude. My contribution to this patent was in development of fine damping concept and development of general timing rules for the nonlinear damping. During the development of the fine nonlinear damping it became apparent that the biggest problem lays with the large dynamic range. To evaluate feasibility, a development board for nonlinear damping was prepared [16]. Experiments using the board and simulations were done. The main limitation in performance were transducer parasitic resonances. To address this limitation focus shifted back to the linear damping methods, which resulted in the second patent application [17]. This patent focused on adaptive linear damping concepts. My main contribution was in development of inductance scaling tuning concept, which relates also to the next thesis goal. I also developed a Direct Iterative Tuning (DIT) concept that is very effective in terms of finding the ideal shunt value, but, rather ineffective in terms of required time. All these methods provide a versatile suite for addressing the damping needs. Thus, I considered the goal to be fulfilled.

Ad 2: The second thesis goal touches the subject of adaptive concepts to improve the ULS performance. Here my contribution was in development and verification of ring-down methods that allow measurement of R_{m0}, f_p, and C_p. The measurement of f_p, and C_p uses an auxiliary inductor. Obviously, all these methods were developed with the intention to make the damping more resilient to the variation in transducer parameters. Specifically, measurement of f_p and C_p was developed as part of adaptive linear damping [17]. Therefore, it was evaluated together with complete adaptive linear damping in chapter 4. Consequently, I would say that the goal was achieved.

Ad 3: After the work on the foundation of the electronic damping the effort continued towards practical design and verifications of the ideas. The key step was to design a necessary hardware for nonlinear and adaptive linear damping. To facilitate future implementation a test chip containing main blocks of coarse nonlinear damping and adaptive linear damping was designed. The nonlinear damping hardware is rather standard consisting of switches and current comparator, and main design challenge being the high voltage. Consequently, it is not that interesting for this thesis, instead the shunt inductance and its scaling property are more interesting. The requirements on the shunt inductance, which is the preferred linear damping solution, are rather challenging. The biggest complication arises from the fact that the inductance must be controlled in extremely wide range (more than two decades) with a rather small step. I was unable to find an existing suitable topology, and thus I proposed new Grounded Inductance Simulator (GIS) topology [18]. The origin of this topology is explained in chapter 3, together with key verification results. Proposed GIS was manufactured on a test chip. Resulting design met all requirements. Therefore, I believe this goal was also achieved.

Ad 4: Final phase of this work focused on bringing together all previous results. To enable this a dedicated test platform was developed [21]. Successful implementation of adaptive linear shunt concept was the first step. The adaptability was nicely demonstrated on the temperature sweep or sweep of parasitic capacitance. The adaptive loop could always find the best possible setting for the inductive shunt. This is thanks to the Indirect Predictive Tuning (IPT) principle [17]. The great advantage of this approach is its fast response that is able to reach the ideal shunt setting just after two or three iterations [20]. To demonstrate the complete concept, the nonlinear damping was added to the system. This assembly shows promising results for the transformer-less systems by reliably achieving minimum distance below 20 cm. The automatic tunning results are comparable with manually found ideal shunt settings. All these findings are described in chapter 4. It is my believe that this achievement can be considered a successful fulfilment of the main thesis objective.

5.1 Future Work

Although the results of damping performance, clearly demonstrated improvements, I must also point out existing limitations, which could be studied and addressed in future. This is the practical realization of tuning of resistive part of linear shunt. The motivation and reasoning are given in chapter 4, nonetheless, this opens possibility of future work.

The assumption significantly simplifies the system, but as was documented in chapter 4, it also presents certain degradation of performance. Although the thesis presented theoretical concepts of adaptive tuning of shunt resistance, none of them were implemented due to their complexity. In this context, the future work could focus

on possibility to optimize the hardware complexity, which is necessary for tuning the shunt resistance.

The next problem relates to a practical implementation of K_{scale} constant, which is influenced by a random across chip variations (mismatch). This variation can impact accuracy of K_{scale}, and thus introduce systematical error to the system. In fact, work on this problem is already ongoing and some results were published [22]. Here I only assisted with the idea formation and helped with the implementation details linked to designed circuitry [18].

REFERENCES

[1] Benchmarking Sensors for Vehicle Computer Vision Systems. *Michigan Tech Research Institute (MTRI)* [online]. Michigan: Michigan Technological University [cit. 2021-10-31]. Available at: https://mtri.org/automotivebenchmark.html

[2] APRI. *APRI - Products - Parking Assistants* [online]. Roznov p. Radhostem: APRI [cit. 2021-08-13]. Available at: https://www.apri.cz/

[3] STEELMATE Automotive. *STEELMATE parking sensors - products* [online]. Dubnica nad Vahom, 2018 [cit. 2021-08-13]. Available at: http://www.steel-mate.eu/

[4] HELLA. *Park Distance Control (PDC): a parking aid based on ultrasound* [online]. HELLA [cit. 2021-08-13]. Available at: https://www.hella.com/

[5] POHL, J, M SETHSSON, P DEGERMAN and J LARSSON. A semi-automated parallel parking system for PASsenger cars. *Proceedings of the Institution of Mechanical Engineers, Part D: Journal of Automobile Engineering* [online]. London: SAGE PUBLICATIONS, 2006, **220**(1), p. 53-65 [cit. 2017-02-26]. ISSN 0954-4070. Available at: doi: 10.1243/095440705X69650

[6] CARULLO, A. and M. PARVIS. An ultrasonic sensor for distance measurement in automotive applications. *IEEE Sensors Journal* [online]. 2001, **1**(2), p. 143-147 [cit. 2021-10-01]. ISSN 1530-437X. Available at: doi: 10.1109/JSEN.2001.936931

[7] JACKSON, J. C., R. SUMMAN, G. I. DOBIE, S. M. WHITELEY, S. G. PIERCE and G. HAYWARD. Time-of-flight measurement techniques for airborne ultrasonic ranging. *IEEE Transactions on Ultrasonics, Ferroelectrics and Frequency Control*. IEEE, 2013, **60**(2), p. 343-355. ISSN 0885-3010. Available at: doi: 10.1109/TUFFC.2013.2570

[8] ADARSH, S, S Mohamed KALEEMUDDIN, Dinesh BOSE and K I RAMACHANDRAN. Performance comparison of Infrared and Ultrasonic sensors for obstacles of different materials in vehicle/ robot navigation applications. *IOP Conference Series: Materials Science and Engineering* [online]. 2016, **149** [cit. 2017-04-24]. ISSN 1757-8981. Available at: doi: 10.1088/1757-899X/149/1/012141

[9] DAI, Hongjun, Shulin ZHAO, Zhiping JIA and Tianzhou CHEN. Low-Cost Ultrasonic Distance Sensor Arrays with Networked Error Correction. *Sensors* [online]. MDPI, 2013, **13**(9), p. 11818-11841 [cit. 2017-04-24]. ISSN 1424-8220. Available at: doi: 10.3390/s130911818

[10] CABRAL, Enrique A. Vargas and Isidro VALDEZ. Airborne ultrasonic sensor node for distance measurement. In: *2013 IEEE SENSORS*. IEEE, 2013, 2013, p. 1-4. ISBN 978-1-4673-4642-9. ISSN 1930-0395. Available at: doi: 10.1109/ICSENS.2013.6688534

[11] HIKITA, Munenori. An introduction to ultrasonic sensors for vehicle parking. *New Electronics: Technology News and Product Design Updates* [online]. MA Business, May 2010 [cit. 2017-02-26]. Available at: http://www.newelectronics.co.uk/

[12] MOHEIMANI, S. O. Reza and Andrew J. FLEMING. *Piezoelectric transducers for vibration control and damping*. London: Springer, 2006. ISBN 978-184-6283-314.

[13] CHERIF, A., M. MEDDAD, A. EDDIAI, A. ZOUHAIR, A. ZAWADZKA and A. MIGALSKA-ZALAS. Multimodal vibration damping using energy transfer. *Optical and*

Quantum Electronics [online]. 2016, **48**(5) [cit. 2017-04-25]. ISSN 0306-8919. Available at: doi: 10.1007/s11082-016-0467-4

[14] MA, Shaodong, Antony J. WILKINSON and Kevin S. PAULSON. An ultrasonic transducer transient compensator design based on a simplified Variable Structure Control algorithm. *Ultrasonics* [online]. 2014, **54**(2), p. 502-515 [cit. 2017-04-26]. ISSN 0041624x. Dostupné z: doi:10.1016/j.ultras.2013.07.017

[15] KOUDAR, Ivan and Jan LEDVINA. *Transducer Controller and Method therefor*. USA. US 10,966,021 B2. Granted 30. 3. 2021. Filled 21. 10. 2015.

[16] LEDVINA, Jan. *Experimentální prototyp pro bez-transformátorové ultrazvukové aplikace* [online]. 2016 [cit. 2021-08-18]. Available at: http://www.urel.feec.vutbr.cz/

[17] KOUDAR, Ivan, Jan LEDVINA, Jiří KUTĚJ and Pavel HORSKÝ. *Piezo Transducer Controller and Method Having Adaptively-Tuned Linear Damping*. USA. US 10,585,178 B2. Granted 10. 3. 2020. Filed 12. 7. 2016.

[18] LEDVINA, Jan and Pavel HORSKÝ. A fully integrated digitally controllable grounded inductor simulator with a large inductance range for damping of ultrasonic transducers. *Analog Integrated Circuits and Signal Processing* [online]. 2020, **102**(1), p. 125-130 [cit. 2020-11-31]. ISSN 0925-1030. Available at: doi: 10.1007/s10470-019-01396-z

[19] FORD, R.L. and F.E.J. GIRLING. Active filters and oscillators using simulated inductance. *Electronics Letters* [online]. 1966, **2**(2) [cit. 2020-11-25]. ISSN 00135194. Available at: doi: 10.1049/el:19660040

[20] LEDVINA, Jan, Lukas VYKYDAL and Pavel HORSKÝ. Fast Automatic Tuning of a Synthetic Inductor for Automotive Transformer-Less Ultrasonic Sensor in Park Assist Systems. *IEEE Sensors Journal* [online]. 2019, **19**(22), p. 10568-10573 [cit. 2021-08-18]. ISSN 1530-437X. Available at: doi: 10.1109/JSEN.2019.2932300

[21] VYKYDAL, Lukáš, and Jan LEDVINA. *Testbed pro metody tlumení měničů s využitím v ultrazvukových parkovacích systémech* [online]. 2019 [cit. 2021-08-18]. Available at: https://www.urel.feec.vutbr.cz/

[22] VYKYDAL, Lukáš, Jan LEDVINA and Pavel HORSKÝ. Dynamic Element Matching for the Grounded Inductor Simulator Output Stage in Ultrasonic Distance Sensor Applications. *IEEE Sensors Letters* [online]. 2020, **4**(8), p. 1-4 [cit. 2021-08-18]. ISSN 2475-1472. Available at: doi: 10.1109/LSENS.2020.3012870

ABSTRACT

A common feature of modern car is a parking assistant that typically depends on performance of ultrasonic sensors. This doctoral thesis opens question of reverberation reduction in these sensors. Reverberation is unwanted phenomenon that prevents the sensor in short distance ranging, which is crucial in a parking application. The thesis intentionally aims on emerging transformer-less sensor solution.

To address the reverberation problem different types of electric damping are studied. From the theory review it became apparent that a combination of multiple damping methods is needed. The proposed practical solution utilizes a nonlinear damping followed by a linear damping. For the linear damping an adaptive shunt tuning method was proposed to address variation in transducer parameters, which enables the system to achieve the fastest damping. To prove viability of this concept a hardware implementing the proposed damping method was developed and using this hardware the methods were evaluated.

ABSTRAKT

Parkovací asistenty jsou dnes běžnou výbavou moderního automobilu. Tato funkce přímo závisí na schopnostech použitých ultrazvukových snímačů. Schopnost měřit krátké vzdálenosti bývá u těchto snímačů omezena reverberacemi (dozvukem). Tyto reverberace jsou nežádoucí jev a tato práce se zabývá možnostmi, jak je potlačit. Záměrně je hledáno řešení pro nově vznikající beztransformátorové snímače.

Pro potlačení reverberací je zapotřebí použití tlumících obvodu. V této práci se probírají zejména elektrické tlumící obvody a metody. Na základě rozboru teorie tlumících metod bylo zjištěno, že praktická realizace bude vyžadovat kombinaci více metod. Kombinace sekvence nelineárního tlumení a lineárního tlumení s automaticky doladěným tlumicím obvodem se jevila jako nejlepší volba. Automatické dolaďování zajišťuje spolehlivě nastavení tlumícího obvodu bez ohledu na rozptyl obvodových parametrů. Navržený koncept byl rovněž obvodově realizován a vlastnosti tlumících metod byly potvrzeny.